A Fully Integrated Micromagnetic Actuator With A Multilevel Meander Magnetic Core

Chong H. Ahn and Mark G. Allen
School of Electrical Engineering
Microelectronics Research Center
Georgia Institute of Technology
Atlanta, GA 30332-0250

ABSTRACT

A fully integrated micromagnetic actuator with a multilevel meander magnetic core is presented. To generate and to confine a magnetic flux in the magnetic core and at the same time minimize coil series resistance, low-resistance meander conductors located in a single plane were interwoven with multilevel meander magnetic cores. This 'wrapped' solenoid (with the core wrapped around the conductor) was fabricated in a fully integrated fashion. A micromagnetic actuator was realized by incorporating a surface micromachined nickel-iron cantilever beam as part of the magnetic circuit of the core. The nickel-iron cantilever beam was 2.5 μm thick, 25 μm wide and 780 μm long, and the magnetic circuit contained 17 turns of meander type solenoid coils. Tip deflection of 4 μm in the vertical direction was achieved when a DC voltage less than 1V (and resulting drive current of 600 mA) was applied to the coils. This fully integrated multilevel topology offers a variety of micromagnetic applications, which can be fabricated on the same substrate with an integrated circuit and actuated with low voltages.

INTRODUCTION

Recently there has been much work towards realizing practical magnetic-based microactuators for variety of applications. These efforts have used hybrid techniques either to place magnetic components onto integrated planar coils [1,2], or to introduce external magnetic fields onto integrated high-permeability moving parts [3]. One reason that these approaches have been taken is due to the difficulty in fabricating three dimensional solenoid type coils using a planar fabrication process. In this work we describe a new 'meander' actuator geometry which is particularly useful in the integrated fabrication of micromagnetic actuators (MMAs).

The major limitations in miniaturization of MMAs arise from poor scaling, difficulty in fabrication, and relatively high resistive losses [4], leading to relatively low actuation efficiencies. However, the usefulness of MMAs depends strongly on the application [1,5]. For example, automotive applications may require much less actuation efficiency than implantable biomedical applications. In addition, MMAs may be the only available microactuation scheme in some cases, including dust-filled environments, operation in conducting fluids, and operation in environments where high driving voltages are unacceptable or unattainable. Since magnetic actuators are current-controlled, they can in theory be operated even at low voltages, which can be obtained from conventional power sources without extra circuits for high voltage generation (of course, maximum current output and slew rate rather than maximum voltage output and slew rate become the controlling power supply issues). In addition, magnetic forces may be more suitable in long range actuation [1,5]. Finally, a micromagnetic structure can play a useful role as an electrical power generator as well as a microactuator [6].

To produce a magnetic force at a specific location, micromagnetic actuators should have an inductive component to generate magnetic flux, and a magnetic core to guide the generated flux to the point where actuation takes place. Coils of conductor material are used for flux generation. The major characteristic of these coils must be low resistance, so that micromagnetic actuators can be driven at reasonable voltages and currents, without high heat power consumption due to the resistance of the conductor. This can be achieved by using a good conductor as the coil material, increasing the thickness of the conductor, and/or utilizing conductor geometries which minimize line length. Copper, gold, and aluminum have been used as conductor materials in previous MMA designs. The magnetic core in the MMA plays two roles: first, it is a mechanical component for actuation; second, it is a magnetic component for flux guidance. Nickel-iron permalloy, in particular, displays outstanding characteristics as an MMA core material from the mechanical [7], magnetic [8], and processing viewpoints.

Several types of planar inductive components have been proposed previously [9,10], but the planar geometry alone is not optimal for fully integrated MMAs. The flux generated from the spiral conductors will be spread out through the surface as both parallel and vertical components with respect to the surface [11]. As a result, it is not easy to guide a flux to a required specific point, unless a magnetic core is included as part of the inductor structure. In addition, the relatively long length of spiral conductors required for a large number of turns produces a high conductor resistance. Thus, alternative geometries for MMA realization were investigated.

DESIGN

Consider the inductor geometries shown in Figure 1. In the standard solenoid geometry (Figure 1b), a conductor line is 'wrapped' around a magnetic core to form an inductive component. Such structures can be realized using multilevel metal interconnect schemes to 'wrap' conductor lines around magnetic materials. However, two problems arise from this geometry: first, the electrical via resistance from layer to layer increases the total conductor resistance; second, the total conductor length must be relatively long. However, the same effect can be realized by switching the roles of conductor and core as in Figure 1a; imagine 'wrapping' a magnetic core around a planar conductor line. This geometry can also be realized using multilevel metal interconnect schemes, by interlacing a meander planar conductor with a multilevel meander magnetic core. This meander geometry has two advantages over the standard solenoid geometry. First, there are no electrical vias to add resistance to the conductor coil. Second, the magnetic core is produced on two levels, making it readily available for surface micromachining of movable core actuators. In addition, the leakage flux of the meander geometry is relatively low. The major disadvantage of the meander geometry is that the total core length (and thus the magnetic reluctance of the core) is increased.

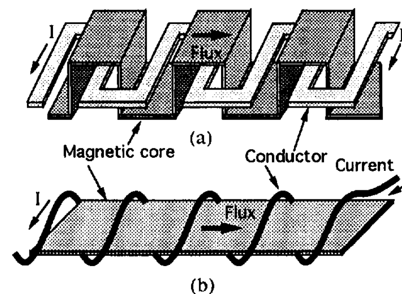

Figure 1. Schematic diagram of a multilevel meander inductive component. (a) schematic diagram of meander type as fabricated (b) analogous structure illustrating the equivalence of 'wrapped' and meander type coils.

0-7803-0456-X/92 $3.00 © 1992 IEEE

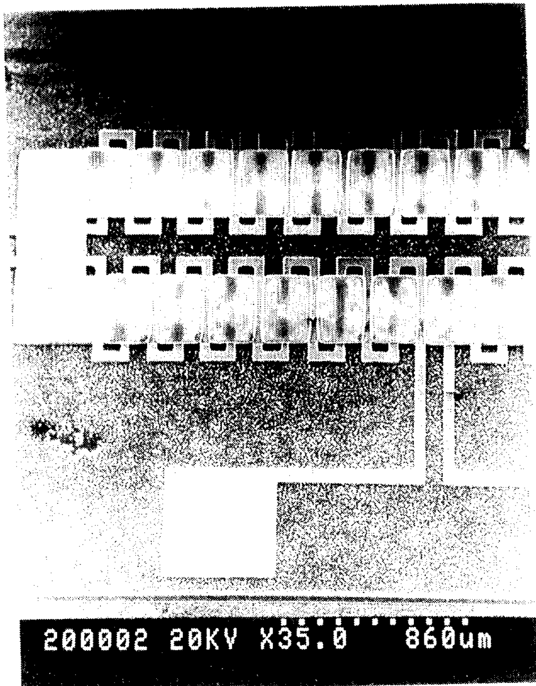

Figure 2. Scanning electron micrograph (SEM) of a fabricated multilevel meander inductor.

In order to demonstrate the feasibility of the meander geometry, a simple inductive structure was designed and fabricated. The fabrication sequence is omitted here due to space considerations, but the strategy is similar to the one described below. Figure 2 shows a scanning electron micrograph of the fabricated multilevel meander inductive component. The inductor structure has 26 turns and a measured inductance of 0.2 μH at a test frequency of 100 kHz. Based on these results, the use of the meander geometry for MMAs was investigated.

By incorporating a surface micromachined nickel-iron cantilever beam as a part of the magnetic core, a fully integrated electromagnetic microactuator can be realized. Figure 3 shows the scanning electron micrograph and a schematic diagram of the integrated MMA. A current through the meander conductors causes the generation of a force of magnetic origin that acts to reduce the total reluctance of the circuit by attracting the released cantilever beam towards the bottom magnetic contact. It should be re-emphasized that a major advantage of the meander geometry is the ease of fabrication of gaps in the magnetic circuit due to the multilevel topology.

ELECTROMECHANICAL MODEL

The magnetic flux that crosses an air gap in a magnetic circuit produces an attractive force between the faces of the magnetic electrodes. The magnetic core structure shown in Figure 3 contains an air gap of variable length g as determined by the position of the movable cantilever beam. If the cantilever beam undergoes a displacement in response to the force of attraction f, the air gap is shortened by the differential length dg, and the work done by the force is the mechanical differential output of the electromagnet

$$d\,W_{mech} = f dg. \tag{1}$$

If the current is adjusted so that the air gap flux remains constant while the gap is shortened by the differential distance dg, the actual force exerted between the faces of the magnetic electrodes is

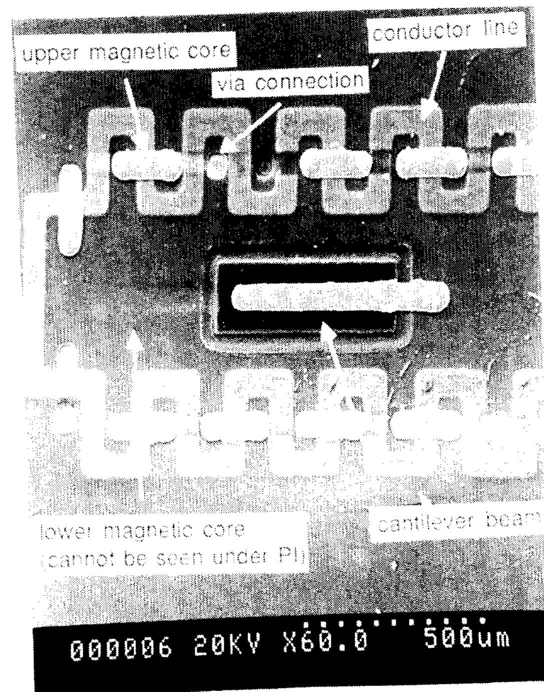

(a)

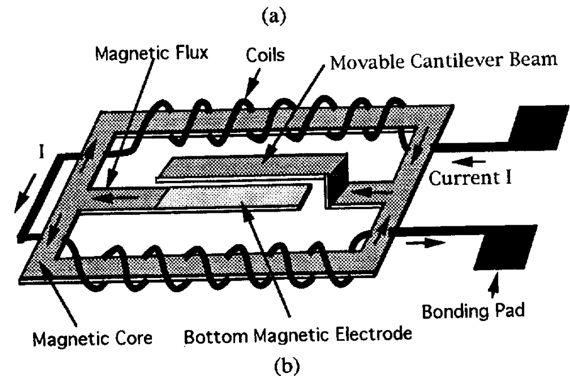

(b)

Figure 3. Scanning electron micrograph (SEM) and schematic diagram of the integrated micromagnetic actuator with nickel-iron cantilever beam. (a) scanning electron micrograph (SEM): magnetic flux is guided both to the cantilever beam and to the bottom magnetic contact. Some upper magnetic core sections have been removed to show the magnetic vias. (b) analogous schematic diagram: the actual meander type coil in the structure is represented as being equivalent to a 'wrapped' solenoid type coil.

$$f = \frac{A_g B_g^2}{2\mu_0}, \tag{2}$$

where μ_0 is the permeability of free space, A_g is the area of the magnetic electrodes, and B_g is the magnetic flux density at the gap.

The paths of magnetic flux and the magnetic equivalent circuit for the designed micromagnetic actuator can be simply drawn from the analogous structure schematic diagram shown in Figure 3b. From Equation (2) and a magnetic equivalent circuit with core length of l_{c1} and N_i turns of coil, the magnetic force

produced in the gap by the current i can be expressed as

$$F_{mag} = \frac{\mu_0 A_g}{2}\left(\frac{N_i i \mu_r A_c}{1.5 l_{c1} A_g + \mu_r y_0 A_c}\right)^2 \quad (N), \qquad (3)$$

where F_{mag} is the force of magnetic origin, μ_r is the relative permeability of the magnetic core which is assumed to be constant (note that this assumes that the core does not saturate), A_c is the area of magnetic core in the inductive component, and y_0 is the initial gap spacing.

A scanning electron micrograph of the nickel-iron cantilever beam released from the surface and its schematic diagram with uniform load q are shown in Figure 4. In some structures, the cantilever beam was designed to have a narrow neck near to the beam support, which tended to increase the flexibility of the beam. In analyzing the bending of these cantilever beam, it was assumed that the width of beam was equal to the width of the neck, since the deflection of the beam would be controlled by the narrow neck.

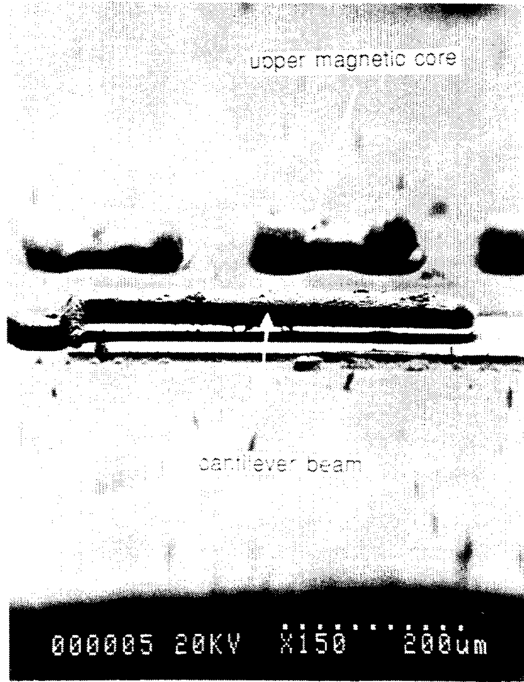

(a)

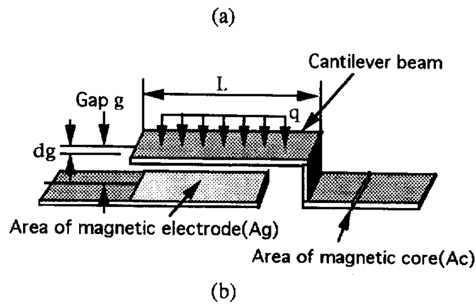

(b)

Figure 4. Scanning electron micrograph of the nickel-iron cantilever beam released from the surface, and a corresponding schematic diagram for the electromechanical model. (a) Scanning electron micrograph of the fabricated nickel-iron cantilever beam; (b) schematic diagram for electromechanical analysis.

Since the size of the gap is small compared to the length of the beam, and since the variation of magnetic reluctance along the length of the beam is small compared to the reluctance of the inductive component, the generated magnetic forces along the cantilever beam are assumed to be constant and are represented as a uniform load q along the cantilever beam in the analysis of mechanical deflection. The load-deflection relationship for a uniformly loaded cantilever beam can be expressed as:

$$q = \frac{8EI\delta_b}{L^4} \quad (N/m), \qquad (4)$$

where δ_b is the deflection of the tip of the cantilever beam, q is the distributed load along the length of the beam, E is the modulus of elasticity of the beam material, and I is the moment of inertia of the beam. Thus, by comparing equations (3) and (4), the relationship between the deflection of the tip of the cantilever beam and the applied current can be expressed as:

$$\delta_b = \frac{\mu_0 A_g}{2}\left(\frac{N_i i \mu_r A_c}{1.5 l_{c1} A_g + \mu_r y_0 A_c}\right)^2 \frac{L^3}{8EI} \quad (m). \qquad (5)$$

FABRICATION

A brief fabrication process of this component is summarized in Figure 5. The process starts with oxidized (0.6 µm) 2-inch <100> silicon wafers as a substrate. Onto this substrate, 2000 Å of titanium was deposited as a electroplating seed layer using DC sputtering. Polyimide (Dupont PI-2611) was then spun on the wafer to build electroplating molds for the bottom magnetic core. Three multi-spin coats were accomplished to obtain a thick polyimide film. Each coat was cast at 3000 rpm, and soft baked

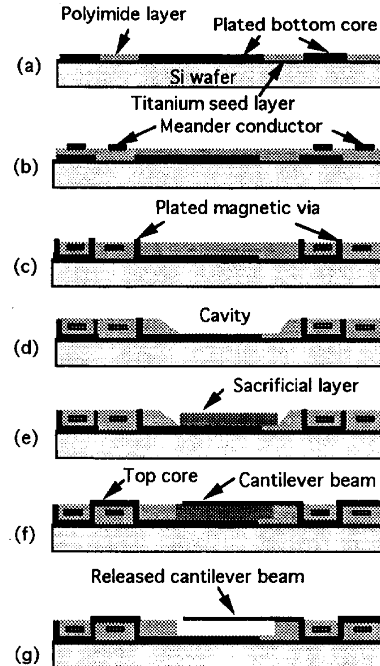

Figure 5. Processing sequence to build a fully integrated micromagnetic actuator. (a) multi-spincoating of polyimide, dry etching, and bottom core plating; (b) patterning of conductor; (c) magnetic via plating; (d) dry etching of cavity; (e) patterning of sacrificial layer; (f) top core and cantilever beam plating; (g) release of cantilever beam.

for 10 minutes at 120 °C prior to the application of the next coat. After deposition of all coats, the polyimide was cured at 350 °C for 1 hour in nitrogen, yielding an after-cure thickness of 9 μm. Holes were etched in this polyimide using a 4% CF_4/O_2 plasma etch and an aluminum hard mask until the titanium seed layer was exposed. The electroplating forms were then filled with nickel (79%) - iron (21%) permalloy using standard electroplating techniques and the nickel-iron electroplating bath described in Table I. To electroplate the bottom magnetic cores, electrical contact was made to the seed layer, and the wafers were immersed in the plating solution. During the electroplating, the solution was maintained at room temperature and a pH of approximately 2.7, and was stirred very slowly with a Teflon propeller blade. An applied current density of 5 mA/cm^2 resulted in a electroplating rate of 0.3-0.4 μm/minute. This rate was chosen as the permalloy was required to be plated exactly up to the top of polyimide mold to achieve a planar surface for subsequent processing.

In order to insulate the bottom magnetic core from the conductor coil, polyimide was spin-coated (as above) at 4000 rpm, and hard-cured at 350 °C for 1 hour. Two different processes were employed to make the conductor coils, one for a deposited aluminum conductor and one for a plated copper conductor. For the aluminum conductor, 5 μm of aluminum was DC sputtered onto the polyimide and patterned using conventional lithography and PAN (phosphoric-acetic-nitric) aluminum etching solution. For the plated copper conductor, copper was plated through a thick photoresist mold. A 2000 Å thick copper seed layer was deposited, and the copper plating mold was formed in 5 μm thick positive photoresist. The copper conductors were plated through the defined molds using standard electroplating techniques and the copper plating solution described in Table I. Note that the bottom magnetic core is electrically isolated from the plating solution during this step. Upon completion of the electroplating, the photoresist was removed with acetone, and the copper seed layer was etched in an HCl-based copper etching solution.

In order to insulate the conductor line and re-planarize the surface, more polyimide was deposited in multiple coats (as described above). Three coats of polyimide were deposited and cured as described above, yielding approximately 9 μm of polyimide. Via holes were then dry-etched through the polyimide layer between the meander conductors using 100% oxygen plasma and an aluminum hard mask. Upon completion of the via etch, the aluminum hard mask was removed. Because the bottom magnetic core was exposed to the oxygen plasma during dry etching, the surface of magnetic core was oxidized. To remove the oxide film, the exposed areas of the bottom magnetic core were etched in a 2% hydrofluoric acid solution for 30 seconds. Contact was then made to the bottom magnetic core and the vias were filled with nickel-iron using the electroplating bath and conditions described previously. Upon completion of the electroplating, the magnetic vias were coated with a single layer of polyimide spun on the wafer at 5000 rpm and cured as described above.

The metal sacrificial layer was then deposited and defined at the desired position of the cantilever beam. A cavity to contain the sacrificial layer was dry-etched down through the polyimide layer using an aluminum mask as described earlier, and the sacrificial layer was buried in this cavity, which improved the planarization of surface for the next process. Two different metals, which could be selectively etched from nickel-iron in a releasing etching solution, were adopted as a sacrificial layer: (1) 7 um thick DC-sputtered Al, or (2) 7 um thick electroplated copper, both deposited as described above. After the patterned sacrificial layer was obtained, the polyimide covering on the magnetic vias was removed by a blanket dry etch. Optionally, additional planarizing steps were performed to fill in areas surrounding the sacrificial layer.

Finally, the top magnetic core and cantilever beam were plated over the magnetic vias and sacrificial layer, completing the magnetic circuit. This was achieved using an evaporated nickel seed layer defined into the desired via and beam shapes using a liftoff technique, a photoresist plating mold, and the electroplating conditions described above. Bonding pads were then opened through polyimide layers for the electrical test by using the via etch process sequence described earlier. Optionally, to remove the titanium plating seed layer located underneath the polyimide, the structure was dry etched to the bottom, and the titanium was then selectively dry etched using a 90% CF_4/O_2 plasma. It should be noted that removal of the magnetic core plating base was not required for successful device performance. Figure 6 shows the side view of the multilevel meander inductive component after this optional removal step has been carried out. Note the magnetic via connecting the top and bottom cores in the meander topology.

After the bonding pads were exposed, the wafer was coated with thick photoresist and patterned to expose the sacrificial layer. The cantilever beams were then released using appropriate selective etches. Approximately 15 minutes of etch time was required to fully release the cantilever beams. After release, the masking photoresist was removed using acetone, and the released structures were rinsed sequentially in DI water, acetone, methanol, and DI water. After rinsing, samples were diced into chips for bonding and test.

Table I. Composition of the nickel-iron and copper electroplating solutions.

Nickel-iron		Copper	
Component	Quantity(g/l)	Component	Quantity
$NiSO_4.6H_2O$	200	$CuSO_4.5H_2O$	1200 (g/l)
$FeSO_4.7H_2O$	8	H_2SO_4	100 (ml/l)
$NiCl_2.6H_2O$	5		
H_3BO_3	25		
Saccharin	3		

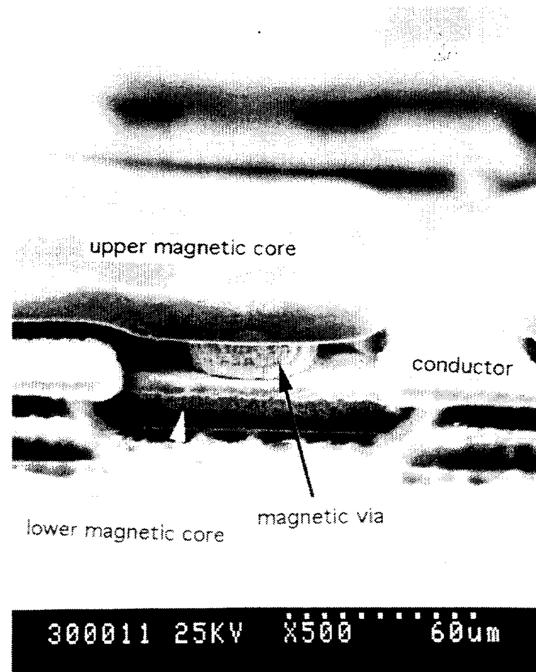

Figure 6. Detailed side view scanning electron micrograph of a magnetic via in the MMA. A magnetic via connecting top and bottom magnetic cores along with a section of conductor is shown.

RESULTS AND DISCUSSION

The chip was bonded and packaged in a standard flat-pack carrier for testing. The deflection of the cantilever beam tip was measured by focusing on the tip of the deflected beam in a Nikon MM-11 Measurescope and measuring the microscope head deflection necessary to maintain focus as the beam deflected. The measured and calculated (equation 5) deflections of the cantilever beam as a function of applied DC current is shown in Figure 7. As expected, the deflection is proportional to the square of current, and the measured results coincide well with the model. The available magnetic force for this microactuator is in the range of 0.1-0.8 µN. The best-fit value for the relative magnetic permeability of this material is approximately 500. This is in good agreement with measured permeabilities of 400-500 which have been measured in test inductive structures using this material.

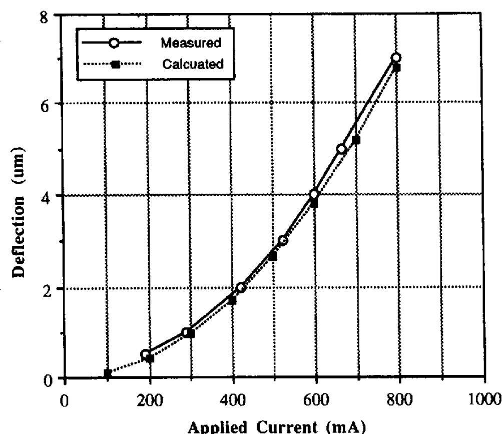

Figure 7. The measured and calculated deflections of the cantilever beam as a function of the applied DC current.

The higher the magnetic permeability that can be achieved, the better the actuator will perform. It has been reported that the permeability of plated nickel-iron magnetic material could be increased up to 5000 by applying 100 Gauss of magnetic field in the direction of easy axis during the plating, and by annealing at a high temperature with magnetic field [12]. If the permeability of the magnetic core can be improved to 2000-5000 in this structure, the available magnetic forces would be in the range of several tens of µN.

One of the claimed advantages of this meander geometry is that the conductor has a relatively small resistance, since the required turns to produce a magnetic flux can be achieved in a short length of conductor without involving any conductor via connections. The resistance of the 17-turn meander conductor in this actuator is measured to be 1.3 ohms at 200 mA. The power consumption due to the conductor resistance at 200 mA is 52 mW.

It was also observed that high current densities could be achieved in the meander conductor. For example, the maximum recommended current density of a conventional magnetic structure in the macro scale at 50 °C has been reported as 5×10^2 A/cm^2 [13]. In the integrated magnetic microactuator, it was verified that the attainable maximum current density ranged from 5×10^4 to 5×10^5 A/cm^2. These values, which are 10^2-10^3 times larger than the values in the macro scale, probably represent the large differences in surface-to-volume ratios of conductors in the macro and micro scale. In addition, since most meander conductors are exposed on or near the surface of the wafer, the generated heat in the conductor can be easily dissipated.

CONCLUSIONS

A fully integrated micromagnetic actuator with a meander coil and multilevel core geometry has been fabricated. Actuation has been realized by incorporating a surface micromachined nickel-iron cantilever beam as a part of the magnetic circuit of the core. Driving voltages of less than one volt and driving currents on the order of several hundred milliamperes resulted in tip deflections of several µm, corresponding to 0.1-0.8 µN of generated magnetic force. The relatively low resistance of the meander conductor results in decreased heat dissipation in the conductor, which increases the efficiency of the device. The low drive voltages make it possible to consider integration of MMAs with IC-based control circuitry.

The allowable maximum current density and power dissipation in this and similar structures should be analyzed in more detail. This will allow experimental evaluation of scaling, power consumption, and other issues of importance in the design of MMAs, and may ultimately illustrate areas of applicability for magnetic microactuators, especially in applications where actuation efficiency is not the primary concern.

ACKNOWLEDGEMENT

This work was supported in part by the National Science Foundation under grant ECS-9117074. The authors would like to thank Mr. Gerald Hill, Mr. Young W. Kim, Mr. A. Bruno Fraizer, and Mr. Bizhan Rashidian of Georgia Tech for valuable technical discussions during the course of this work. The authors would also like to gratefully acknowledge DuPont for their donation of polyimides which have been used in this work.

REFERENCES

[1] B. Wagner and W. Benecke, Microfabricated Actuator with Moving Permanent Magnet, Proc. IEEE Microelectromechanical Systems Workshop, pp. 27-32, 1991.

[2] B. Wagner, M. Kreutzer, and W. Benecke, Linear and Rotational Magnetic Micromotors Fabricated using Silicon Technology, Proc. IEEE Microelectromechanical Systems Workshop, pp. 183-189, 1992.

[3] H. Guckel, K.J. Skrobis, T.R. Christenson, J. Klein, S. Han, B. Choi, E. G. Lovell, and T. W. Chapman, On the Application of Deep X-ray Lithography with Sacrificial Layers to Sensor and Actuator Construction, Proc. 6th International Conference on Solid-State Sensors and Actuators, 1991.

[4] W. S. N. Trimmer, Microbots and Mechanical Systems, Sensors and Actuators, vol. 19, pp. 267-287, 1989.

[5] W. Benecke, Silicon-Microactuators: Activation Mechanism and Scaling Problems, Proc. 6th International Conference on Solid-State Sensors and Actuators, pp. 46-50, 1991.

[6] R. E. Hetrick, A Vibrating Cantilever Magnetic field Sensor, Sensors and Actuators, Vol. 16, pp. 197-207, 1989.

[7] R. D. MacInnis and K. V. Gow, Tensile Strength and Hardness of Electrodeposited Nickel-Iron Foil, Plating, pp. 135-136, Feb. 1971.

[8] M. E. Henstock and E. S. Spencer-Timms, The Composition of Thin Electrodeposited Alloy Films with Special Reference to Nickel-Iron, Proc. 6th International Metal Finishing Conference, pp. 179-185, 1963.

[9] R. F. Soohoo, Magnetic Thin Film Inductors for Integrated Circuit Application, IEEE Trans. on Magnetics, MAG-15(6), pp. 1803-1805, 1979.

[10] O. Oshiro, H. Tsujimoto, and K. Shirae, A Novel Miniature Planar Inductor, IEEE Trans. on Magnetics, MAG-23(5), pp. 3759-3761, 1987.

[11] H. M. Greenhouse, Design of Planar Rectangular Microelectronic Inductors, IEEE Trans. on Parts, Hybrids and Packaging, PHP-10(2), pp. 101-109, 1974.

[12] R. L. Anderson, E. E. Castellani, P. M. McCaffrey, and L. T. Romankiw, Method for Treating Magnetic Alloy to Increase the Magnetic Permeability, United States Patent #4,003,768

[13] C. W. T. McLyman, Transformer and Inductor Design Handbook, pp. 66-72, Marcel Dekker Inc., New York, 1978.